# Techno-economic Optimization of Flywheel Storage System in transportation

Jean-Christophe Olivier, Nicolas Bernard, Sony Trieste, Luis Mendoza, Salvy Bourguet

# Techno-economic Optimization of Flywheel Storage System in transportation

J.C. Olivier, N. Bernard, S. Trieste, Salvy Bourguet, L. Mendoza Aranguren
Laboratoire IREENA, Saint-Nazaire

**ABSTRACT – Energy storage technologies in transport applications are continuously improved and updated to ensure energy demand, to decrease the fuel consumption and in order to make systems more reliable. Flywheel kinetic energy storage offers very good features such as power and energy density. Moreover, with some short-range vehicles such as buses or small ferries, this technology can be enough to supply all the energy to the power train.The challenges to be met to integrate such technology in vehicles are the mass, the efficiency and especially the cost. Then, in this paper, a techno-economic optimization of a flywheel energy storage system is presented. It is made up of a flywheel, a permanent magnet synchronous machine and a power converter. For each part of the system, physical and economical models are proposed. Finally, an economic optimization is done on a short-range ship profil, currently using supercapacitors.**

***KEYWORDS – Techno-economic analysis, energy storage, transportation, flywheel.***

## 1. INTRODUCTION

Flywheel kinetic energy storage offers very good features such as power and energy density[1, 2]. Moreover, they have long lifetime in comparison to classical electrochemical storage systems. In transportation applications, high-speed flywheels as energy storage system has been largely neglected compared to other technologies such as ultracapacitors or batteries [3]. Indeed, many studies show that the flywheel is a mature energy storage technology and competitive with common storage systems [4, 5, 6], even if there is strong security constraints for such storage technology, especially for transportation applications where significant gyroscopic effects may occur [5]. The design of a flywheel is then relatively complex and must take into account many subparts and devices. Indeed, it is composed of the flywheel itself, but also of the electrical machine for electromechanical conversion, power converter to control the power flows, magnetic bearings and vacuum enclosures to reduce aerodynamic and mechanical frictions losses. It is then obvious that the optimization of such a system requires a thorough and complete modeling of all these elements.

This paper proposes a comprehensive techno-economic modeling of a flywheel energy storage system. The bulk of this work is based on an optimization of the flywheel, the electrical machine and the power converter as a whole. In this work, magnetic bearings and vacuum enclosures are not taken into account and are seen as auxiliaries. Indeed, both devices have little influence on the system design and a high cost due to there high value-added. So, their cost and mass can be determined independently and more especially for magnetic bearings.

To be more representative of the use of storage systems, the optimization is not done on one typical torque-speed operating point but on an operating profile [7, 8, 3]. Applying this approach to transportation applications, it is proposed to explore best set of tradeoff between cost and size of the system (Pareto front), for different materials of the flywheel. In this paper, the techno-economic optimization is applied on an electric ship currently using supercapacitors as the primary source of energy [9, 10, 11]. The paper is organized as follow. In section 2, the studied flywheel storage system is presented as well as the load profil. Physical and electrical models, useful for the design of each subpart of the FSS, are given by section 3. Economical models are given by section 4. These models concern the acquisition and the operation cost of each device in the power chain. With these models, section 5 presents the optimization results, obtained on the full-electric ship *Ar Vag Tredan*. Conclusion is given in section 6.

## 2. STRUCTURE OF THE FLYWHEEL SYSTEM AND LOAD PROFILE

The studied flywheel storage system (FSS) is composed of a rotating mechanical part (the flywheel), a permanent magnet synchronous machine (PMSM) and an IGBT power converter (see Fig 1). The choice of the technology of each part of this system will be discussed and justified in the final paper [6, 3, 12, 7, 2, 13, 14].

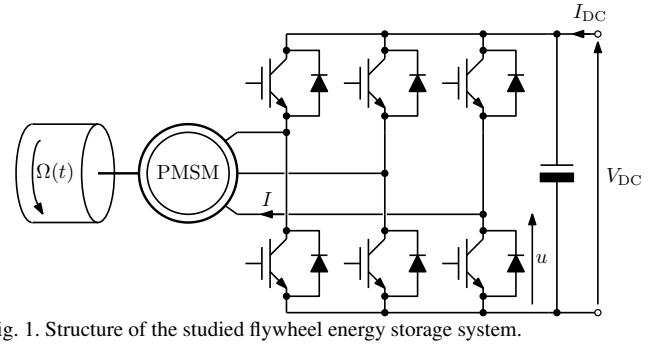


Fig. 1. Structure of the studied flywheel energy storage system.

## 3. PHYSICAL MODELS AND LOSSES

In this section, the physical models of each part of the flywheel storage system are presented. These models include the sizing and the losses calculation. A special attention is payed to the permanent magnet synchronous machine, which is the critical element of such a system. Indeed, it is the interface between the mechanical energy stored is the flywheel and the electrical power train. In this paper, an original analytical sizing of PMSM is presented, taken into account the power and speed profile of the flywheel [7].

### 3.1. *Flywheel*

The mechanical energy is classically stored in a rotating mass, made of steel or composite material. The total energy $W$, stored in a flywheel is expressed by the well known equation

$$W = \frac{1}{2} J \Omega^2 \tag{1}$$

where $J$ is the moment of inertia ($\mathrm{kg.m^2}$) and $\Omega$ is the angular velocity (rad/s). Because a flywheel storage system use an electromechanical conversion, the total stored energy can not be used. Indeed, a minimal angular velocity $\Omega_{\min}$ must be defined. The expression of exploitable energy becomes :

$$W_{exp} = \frac{1}{2} J (\Omega^2 - \Omega_{\min}^2) \tag{2}$$

Classical values for $\Omega_{\min}$ are between 40 to 60 % of the maximal angular velocity [6]. It permit to obtain respectively 85 and 65 % of the stored energy. Concerning the moment of inertia $J$, It is possible to rewrite it from the mass and shape of the flywheel. For steel rotors, the dominant shape is the hollow cylinder [1], whose inertia expression is given by

$$J = \frac{1}{4} m_{\mathrm{fw}} (R_{\mathrm{fw}}^2 - (r_{\mathrm{i}} R_{\mathrm{fw}})^2) = \frac{1}{4} m_{\mathrm{fw}} R_{\mathrm{fw}}^2 (1 - r_{\mathrm{i}}^2) \tag{3}$$

where $m$ is the mass (kg), and $R_{\mathrm{fw}}$ and $R_{\mathrm{i}}$ are respectively the outer and inner radius, as shown in figure 2. For more convenience, the inner radius $R_{\mathrm{i}}$ can be expressed by its dimensionless value $r_{\mathrm{i}}$. From equations (1) and (3), it is clearly seem that the simplest way to increase the stored energy is speeding up the flywheel.

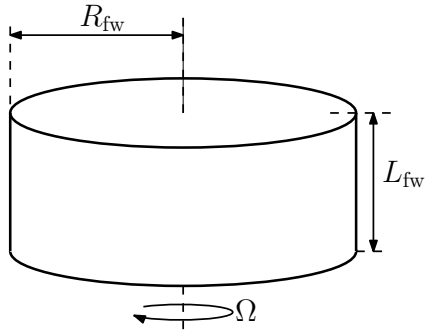


Fig. 2. Flywheel cylinder.

But for a given material, the tensile strength $\sigma$ limit the maximum peripheral speed $v_{\mathrm{p\,max}}$ (in $\mathrm{m.s^{-1}}$). Regarding this constraint, a maximum energy density is obtained and given by

$$e_m = K \frac{K_{\mathrm{s}}\, \sigma}{\rho} \tag{4}$$

where $K$ is the shape factor of the flywheel, $K_{\mathrm{s}}$ a mechanical security factor and $\rho$ the mass density of the material. It is also possible to calculate the maximum peripheral speed $v_{\mathrm{p\,max}}$ with the next equation :

$$v_{\mathrm{p\,max}} = R_{\mathrm{fw}}\, \Omega_{\max} = \sqrt{\frac{K_{\mathrm{s}}\, \sigma}{K\, \rho}} \tag{5}$$

The shape factor $K$ only depends on the flywheel geometry. For a plain cylinder, it is equal to 0.606 and tends towards 0.5 for a hollow cylinder [3]. Now that the basic equations are given, it is possible to design a flywheel according to two main data :

- The inertia $J$ of the flywheel,
- the maximal angular velocity $\Omega_{\max}$ (rad/s),

From equation (5) and knowing the mechanical parameters of the flywheel material, it is possible to deduce the outer radius $R_{\mathrm{fw}}$ given at figure 2. Next, for a given inner radius ratio $r_{\mathrm{i}}$, the length of the flywheel $L_{\mathrm{fw}}$ is deduce from equation (3) and its shape. Finally, the geometrical parameters of an allow cylinder are given by :

$$R_{\mathrm{fw}} = \frac{1}{\Omega_{\max}} \sqrt{\frac{\sigma}{K\, \rho}} \tag{6}$$

$$L_{\mathrm{fw}} = \frac{4\, J}{\rho\, \pi\, R_{\mathrm{fw}}^2\, (1 - r_{\mathrm{i}}^2)} \tag{7}$$

In the case of a plain cylinder with a null inner radius ($r_{\mathrm{i}} = 0$), the geometrical parameters of the flywheel are given by the two next equations :

$$R_{\mathrm{fw}} = \frac{1}{\Omega_{\max}} \sqrt{\frac{\sigma}{K\, \rho}} \tag{8}$$

$$L_{\mathrm{fw}} = \frac{4\, J}{\pi} \left( \frac{\Omega_{\max}^2\, K\, \rho}{\sigma} \right)^2 \tag{9}$$

### 3.2. *Permanent magnet synchronous machine*

In this section, the permanent magnet synchronous machine is sized from an optimized analytical approach developed in [7] and [12]. With this model the geometry of the machine is obtained taken into account mechanical and thermal constraints, core and copper losses. The optimization criterion is the specific power. This methodology is applied and generalized to arbitrary torque and speed profiles. The geometry of the machine is illustrated by figure 3.

In this model, it is assume that the steel parts are infinitely permeable, the study is limited to the first harmonic and the losses in permanent magnets, due to the slot effects, are neglected. At last, the thermal constraint consist on a maximal temperature increase between the winding and the external surface (constant during a time cycle). For a stator field considered in quadrature with the

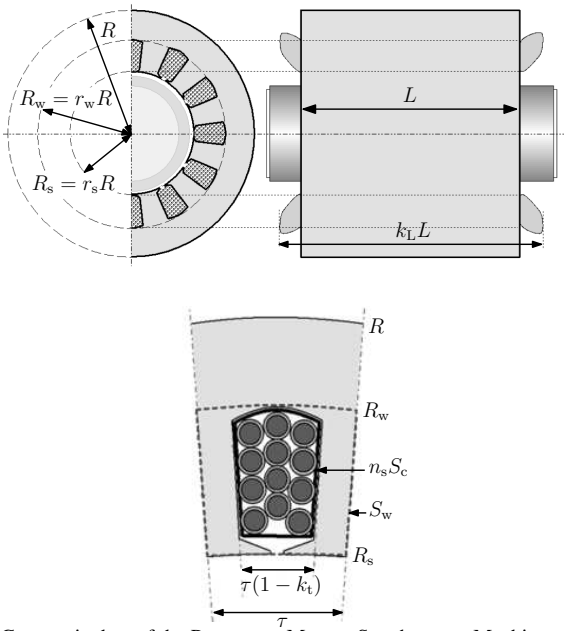

Fig. 3. Geometric data of the Permanent Magnet Synchronous Machine.

rotor field, and for a sinusoidal distribution, the electromagnetic power is given by

$$P_{\rm em}(t) = \frac{12}{\sqrt{2}} R_{\rm s}\, L\, B_{\rm fm} F_{\rm s}\, p\, \Omega(t) \tag{10}$$

where $F_{\rm s}$ is the magnetomotive force (in A.t) created by one phase, $B_{\rm fm}$ the magnitude of the radial magnet flux density (in T) and $p$ the number of pole pairs.

### 3.2.1. *Thermal constraint*

So, considering an average heat transfer coefficient $h$ and a temperature rising $\Delta T_{\rm max}$, the thermal constraint is given by

$$\Delta T_{\rm max} = \frac{1}{h\, S_{\rm th}} \frac{1}{T_{\rm cyc}} \int_0^{T_{\rm cyc}} P_{\rm losses}(t)\, dt \tag{11}$$

where $T_{cyc}$ is the charge-discharge cycle duration of the flywheel (in s), $P_{\rm losses}$ is the sum of copper and core losses (in W) and $S_{\rm th}$ is the surface area of convective heat transfer (in $m^2$), given by

$$S_{\rm th} = 2\,\pi\, R\,(R + L) \tag{12}$$

In fact, assuming a constant temperature rising on the cycle, the thermal constraint only depends on the average losses of the machine.

### 3.2.2. *Losses calculation*

For the copper losses, there are given from the stator magnetomotive force $F_{\rm s}$ and from geometrical parameters [7] :

$$P_{\rm co} = \frac{144}{\pi} \rho_{\rm co} \left(\frac{k_{\rm L}\, L}{k_{\rm f}}\right) \frac{p^2}{R_{\rm w}^2 - R_{\rm s}^2} F_{\rm s}^2 \tag{13}$$

with $\rho_{\rm co}$ the electric resistivity, $k_{\rm f}$ the winding fill factor, and where $k_{\rm L}$, $L$, $R_{\rm w}$ and $R_{\rm s}$ are the geometrical parameters shown in figure 3. Expressing the winding fill factor $k_{\rm f}$ in terms of filling factor per slot $k_{\rm f0}$, we have :

$$k_{\rm f} = k_{\rm f0}\,(1 - k_{\rm t}) \tag{14}$$

From equation (10), the magnetomotive force $F_{\rm s}$ can be rewrite from the electromagnetic torque :

$$F_{\rm s}(t) = \frac{\Gamma_{\rm em}(t)}{\alpha\, B_{\rm fm}} \tag{15}$$

where

$$\alpha = \frac{12}{\sqrt{2}}\, p\, R_{\rm s}\, L \tag{16}$$

For the core losses, the principle of losses separation (hysteresis and eddy current) [15, 16] or the Steinmetz relationship [17] can be both considered. But insofar as the average losses must be calculated, the use of fractional powers add complexity in the calculation. It is the reason why the losses separation method is used in this work. Here, losses in the yoke $P_{\rm mgy}$ and in the teeth $P_{\rm mgt}$ are considered. Using the Gauss law, the induction in these respective parts are given by

$$B_{\rm y} = \frac{1}{p} \frac{R_{\rm s}}{R - R_{\rm w}} B_{\rm fm} \tag{17}$$

$$B_{\rm t} = \frac{1}{k_{\rm t}} B_{\rm fm} \tag{18}$$

and the volume of the yoke $V_{\rm y}$ and the theeth $V_{\rm t}$ are

$$V_{\rm y} = \pi\,(R^2 - R_{\rm w}^2)\, L \tag{19}$$

$$V_{\rm t} = k_{\rm t}\pi\,(R_{\rm w}^2 - R_{\rm s}^2)\, L \tag{20}$$

Finally, from equation (17) to (20), with the separation losses principle, the total core losses $P_{\rm mg}$ in the yoke and teeth are given by

$$P_{\rm mg}(t) = k_{\rm ad}\left(k_{\rm ec}\, p^2 \Omega^2(t) + k_{\rm h}\, p\, \Omega(t)\right)\, V_{\rm ol}\, B_{\rm fm}^2 \tag{21}$$

where $k_{\rm ad}$ is an additional factor which permits to take into account the defects in materials and manufacturing processes and $V_{\rm ol}$ the equivalent volume

$$V_{\rm ol} = V_{\rm y} \left(\frac{1}{p} \frac{R_{\rm s}}{R - R_{\rm w}}\right)^2 + V_{\rm t} \frac{1}{k_{\rm t}^2} \tag{22}$$

Now, copper losses given by equation (13) and core losses given by equation (21) can be solved on one flywheel cycle, according to the thermal constraint (11). Average value of the copper losses is

$$P_{\rm co(avg)} = \frac{1}{T_{\rm cyc}} \int_0^{T_{\rm cyc}} \frac{\beta}{\alpha^2\, B_{\rm fm}^2} \Gamma_{\rm em}^2(t) dt \tag{23}$$

which is also the calculation of the r.m.s torque value :

$$P_{\rm co(avg)} = \frac{\beta}{\alpha^2\, B_{\rm fm}^2} \Gamma_{\rm em(rms)}^2 \tag{24}$$

where $\beta$ is given by

$$\beta = \frac{144}{\pi} \rho_{\rm co} \left(\frac{k_{\rm L}\, L}{k_{\rm f}}\right) \frac{p^2}{R_{\rm w}^2 - R_{\rm s}^2} \tag{25}$$

In the same way, the average value of core losses can be expressed in the form

$$P_{\mathrm{mg(avg)}} = k_{\mathrm{ad}} \left( k_{\mathrm{ec}}\, p^2 \Omega^2_{\mathrm{(rms)}} + k_{\mathrm{h}}\, p\, \Omega_{\mathrm{(avg)}} \right) V_{\mathrm{ol}}\, B^2_{\mathrm{fm}} \quad (26)$$

### 3.2.3. *Mechanical constraint*

In electrical machines, the mechanical constraints are mainly due to centrifugal forces (which impose a maximum peripheral speed $v_{\mathrm{pm(lim)}}$) and to the first natural frequency of the rotor [18, 19]. Considering a typical value of the peripheral speed (close to 150 rad/s), the limitation is only due to the ratio between the length and the rotor radius [18, 7], such as

$$\tau_{\mathrm{L}} = \frac{L}{R_{\mathrm{s}}} \leqslant 5 \quad (27)$$

It can be notice that once the optimal sizing result is obtained (c.f. section 3.2.4), the maximum peripheral speed should be checked to verify that it is lower than $v_{\mathrm{pm(max)}}$.

### 3.2.4. *Sizing optimization*

From the thermal constraint given by equation (11), the first optimization consists to the losses minimization for a given sizing. Considering equations (24) and (26) and by defining the following expressions :

$$\beta_0 = \frac{\beta}{\alpha^2} \Gamma^2_{\mathrm{em(rms)}} \quad (28)$$

$$\gamma_0 = k_{\mathrm{ad}} \left( k_{\mathrm{ec}}\, p^2 \Omega^2_{\mathrm{(rms)}} + k_{\mathrm{h}}\, p\, \Omega_{\mathrm{(avg)}} \right) V_{\mathrm{ol}} \quad (29)$$

it result that the losses expression becomes :

$$P_{\mathrm{losses(avg)}} = \gamma_0 B^2_{\mathrm{fm}} + \frac{\beta_0}{B^2_{\mathrm{fm}}} \quad (30)$$

Therefore, the losses minimization gives

$$B_{\mathrm{fm(opt)}} = \left( \frac{\beta_0}{\gamma_0} \right)^{1/4} \quad (31)$$

that is to say when the copper losses and the core losses are equal. It gives for the losses expression, according to the thermal constraint (11) :

$$P_{\mathrm{losses(avg)}} = 2\sqrt{\gamma_0\, \beta_0} = h\, S_{\mathrm{th}} \Delta T_{\max} \quad (32)$$

Then, using equations (28), (29), (24), (22) and (13), the volume of the machine is expressed by

$$\begin{aligned} V_{\mathrm{PMSM}} = \; & \sqrt{2}\, \frac{\Gamma_{\mathrm{em(rms)}}}{h\, \Delta T_{\max}} \times \frac{L/R}{1 + L/R} \times \sqrt{\frac{\rho_{\mathrm{co}}\, k_{\mathrm{L}}}{k_{\mathrm{f}}}} \\ & \times \sqrt{\frac{k_{\mathrm{ad}} \left( k_{\mathrm{ec}}\, p \Omega^2_{\mathrm{(rms)}} + k_{\mathrm{h}}\, \Omega_{\mathrm{(avg)}} \right)}{p}} \\ & \times \sqrt{\frac{1 + r_{\mathrm{w}}}{(1 - r_{\mathrm{w}})\,(r^2_{\mathrm{w}} - r^2_{\mathrm{s}})} + \frac{p^2}{k_{\mathrm{t}}\, r^2_{\mathrm{s}}}} \end{aligned} \quad (33)$$

Then, to optimize the specific power of the machine, the volume given by (33) must be minimized through the geometrical parameters $r_{\mathrm{w}}$, $r_{\mathrm{s}}$ and the number of pole pairs $p$. In [7], it is demonstrate that the optimal design for an Si.Fe stator core is obtained with the next parameter set (for speed above 3000 rpm) :

$$p = 1; \quad r_{\mathrm{s}} = 0.44; \quad r_{\mathrm{w}} = 0.73 \quad (34)$$

From the volume equation (33) and for a given ratio $\tau_{\mathrm{rl}} = L/R$, all the mechanical and electrical parameters of the machine can be computed. The length $L$ and the external radius $R$ are given by

$$R = \left( \frac{V_{\mathrm{PMSM}}}{\pi\, \tau_{\mathrm{lr}}} \right)^{1/3} \quad (35)$$

$$L = \tau_{\mathrm{lr}}\, R \quad (36)$$

In the same way, the maximal peripheral speed can be calculated and must be compared to those given by the tensile strength limit :

$$V_{\mathrm{pm(max)}} = \left( \frac{V_{\mathrm{PMSM}} \Omega^3_{(max)}\, r^2_{\mathrm{s}}}{\pi\, \tau_{\mathrm{lr}}} \right)^{1/3} < v_{\mathrm{pm(lim)}} \quad (37)$$

### 3.2.5. *Electrical parameters and mass*

The equations (33), (35) and (36) permit to calculate the electrical parameters and the quantity of magnet, iron and copper of the machine. The electrical model of the machine given by figure 4 take into account the induced electromotive force $E(t)$ (in V), the terminal resistor of the winding $R_{\mathrm{co}}$ (in $\Omega$) and the cyclic inductance $L_{\mathrm{cyc}}$ (in H). The terminal resistor $R_{\mathrm{co}}$ and the cyclic inductance can be obtained from the geometrical parameters of the machine :

$$R_{\mathrm{co}} = \frac{144}{3\,\pi} \frac{\rho_{\mathrm{co}}\, k_{\mathrm{L}}\, \tau_{\mathrm{L}}\, R}{k_{\mathrm{f}}} \frac{p^2\, n^2}{R^2_{\mathrm{w}} - R^2_{\mathrm{s}}} \quad (38)$$

$$L_{\mathrm{cyc}} = \frac{6\,\pi\,\mu_0\, n^2\, R_{\mathrm{s}}\, L}{e + e_{\mathrm{mag}}} \quad (39)$$

$$E(t) = k_\phi \Omega(t) \quad (40)$$

$$k_\phi = \frac{4}{\sqrt{2}}\, B_{\mathrm{opt}}\, R_{\mathrm{s}} L\, n\, p \quad (41)$$

with $n$ the turns number, $\mu_0$ the vacuum permeability, $e$ the mechanical airgap and $e_{\mathrm{mag}}$ the height of the magnets.

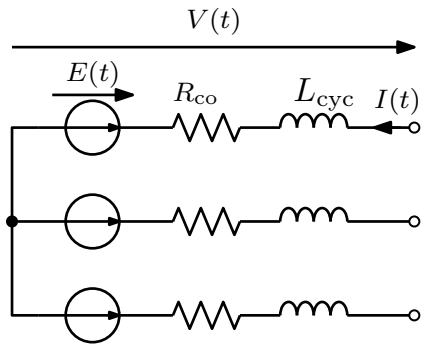


Fig. 4. Electrical model of the Permanent magnet synchronous machine.

Now, let us define the total iron mass of the machine. From the geometrical parameters illustrated by figure 3, the iron mass is calculated from the yooke ($V_{\rm y}$) and theeth ($V_{\rm th}$) volumes given by equations (19) and (20), and from the rotor volume

$$V_{\rm r} = \pi \left(R_{\rm s} - e - e_{\rm mag}\right)^2 L \tag{42}$$

Knowing the mass density of iron ($\rho_{\rm iron}$), the total mass is given by :

$$m_{\rm iron} = \rho_{\rm iron} \left(V_{\rm r} + V_{\rm y} + V_{\rm t}\right) \tag{43}$$

The total cooper mass is also obtain from the geometrical parameters (c.f. figure 3) and is given by :

$$m_{\rm co} = \rho_{\rm co}\, k_{\rm w}\, \pi \left(1 - k_{\rm t}\right) \left(R_{\rm w}^2 - R_{\rm s}^2\right) k_{\rm l}\, L \tag{44}$$

with $\rho_{\rm co}$ the mass density of copper and $k_{\rm w}$ the slot fill factor.

Finally, the magnet mass is defined to ensure the needed flux density $B_{\rm ag}$ in the airgap. The optimal volume of magnet is obtained from the Evershed criterion [20], which impose a magnet thickness equal to the airgap $e$. In this case, the flux density $B_{\rm ag}$ is the half of the remanent flux density $B_{\rm r}$ of the magnet. Then, as shown in figure 5, the magnitude of the first harmonic $B_{\rm fm(opt)}$ given by equation (31) is obtained from the magnet flux density $B_{\rm r}$ and from the magnet pole arc $\theta_{\rm mag}$ :

$$B_{\rm fm(opt)} = \frac{4}{\pi} \frac{B_{\rm r}}{2} \sin\left(p \frac{\theta_{\rm mag}}{2}\right) \tag{45}$$

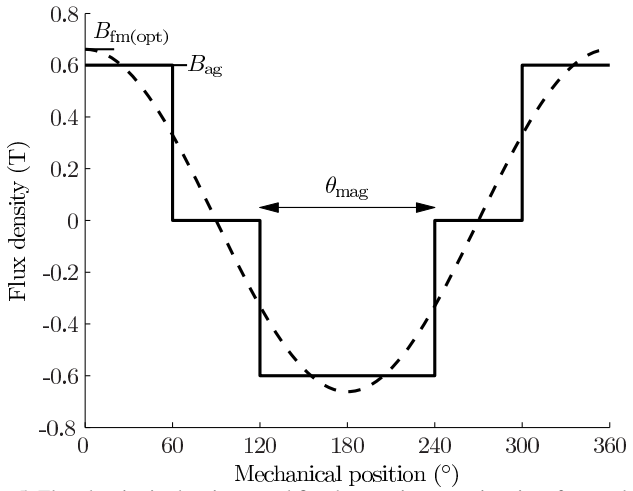


Fig. 5. Flux density in the airgap and first harmonic approximation, for a pole pair $p = 1$, a magnet thickness $e_{\rm mag} = e$, an magnet pole arc $\theta_{\rm mag} = 120°$ and a remanent flux density $B_{\rm r} = 1.2\,{\rm T}$.

Knowing the air gap $e$ and the flux densities $B_{\rm r}$ and $B_{\rm fm(opt)}$, the magnet pole arc is given by

$$\theta_{\rm mag} = \frac{2}{p} \arcsin\left(\frac{\pi}{2} \frac{B_{\rm fm(opt)}}{B_{\rm r}}\right) \tag{46}$$

From these geometrical parameters, the total mass of magnet is given by :

$$\begin{aligned} m_{\rm mag} &= \rho_{\rm mag} \theta_{\rm mag} p \left((R_{\rm s} - e)^2 - (R_{\rm s} - e - e_{\rm mag})^2\right) L \\ &= \rho_{\rm mag} \theta_{\rm mag} e_{\rm mag} p \left(2R_{\rm s} - 2e - e_{\rm mag}\right) L \end{aligned} \tag{47}$$

where $\rho_{\rm mag}$ is the mass density of magnet.

### 3.3. *Power converter*

In this section, the design and sizing of the power electronic converter is presented. It is used to control power flows between the FESS and the loads. The structure of this power converter is three-phases IGBT bridge, as shown in figure 8. The loads are connected to the DC side, as well as the power supply used to recharge the flywheel. The PMSM is connected to the AC side of this converter. The used convention for the machine is a positive power during the recharge of the flywheel, i.e. a negative power during its discharge.

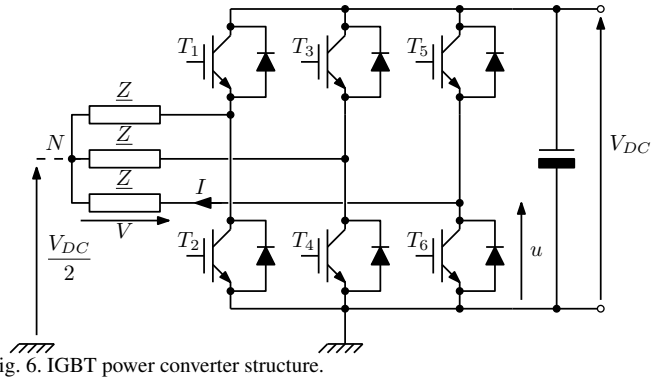


Fig. 6. IGBT power converter structure.

The topology of such a device consists in two IGTB and two parallel diodes per branch and the control is assumed to be a classical symetric PWM. During a period $T$ of pulse-width modulation (PWM), the transistors $T_{1,3,5}$ operate throughout the time $a\,T$, where $a$ is the duty cycle. On the contrary, transistors $T_{2,4,6}$ will operate during the time $(1 - a)\,T$. Therefore, the average voltage $u(t)$ applied to each phase of the power converter can be written as follows :

$$u(t) = a(t)\, V_{\rm DC} \tag{48}$$

where $V_{\rm DC}$ is the voltage value of the DC-bus. The voltage $V(t)$ applied to each phase of the PMSM is then given by

$$V(t) = \left(a(t) - \frac{1}{2}\right) V_{\rm DC} \tag{49}$$

with a variable changing $a(t) - 1/2 = m(t)$, it is possible to express the PMSM phase voltage $V(t)$ such as :

$$V(t) = m(t)\, \frac{V_{\rm DC}}{2} \tag{50}$$

In this work, the three voltages $V(t)$ and currents $I(t)$ of the PMSM are considered sinusoidal and balanced :

$$V(t) = V_{\rm m} \sin(\omega t - \phi_{\rm v/i}) \tag{51}$$

$$I(t) = I_{\rm m} \sin(\omega t) \tag{52}$$

where $\phi_{\rm v/i}$ is the phase shift between the voltage $V(t)$ and the current $I(t)$ and where $V_{\rm m}$ and $I_{\rm m}$ are respectively the voltage and current magnitude. From equations (50) and (51), the modulation index $m(t)$ can be expressed as a function of $V(t)$, such

as

$$m(t) = \frac{2\,V_{\rm m}}{V_{\rm DC}}\,\sin\left(\omega\,t-\phi_{\rm v/i}\right) \quad (53)$$

$$a(t) = \frac{V_{\rm m}}{V_{\rm DC}}\,\sin\left(\omega\,t-\phi_{\rm v/i}\right)+\frac{1}{2} \quad (54)$$

### 3.3.1. *Power losses calculation*

Now, the dissipated power in each IGBT transistors during the conduction state must be determined. A classical result of a full IGBT bridge losses expression is given by [13, 14, 21] :

$$\begin{aligned} P_{\rm igbt} &= 6\,\frac{\omega}{2\,\pi}\int_0^{\pi/\omega} a(t)\,\left(V_{\rm ce0}\,I(t)+R_{\rm c}\,I^2(t)\right)\,dt \\ &= 3\,I_{\rm m}\left(\frac{V_{\rm ce0}}{\pi}+\frac{R_{\rm c}\,I_{\rm m}}{4}\right) \\ &+ \frac{V_{\rm m}I_{\rm m}}{V_{\rm DC}}\cos(\phi_{\rm v/i})\left(\frac{V_{\rm ce0}}{8}+\frac{R_{\rm c}I_{\rm m}}{3\,\pi}\right) \end{aligned} \quad (55)$$

In the same way, considering a conductive resistance $R_d$ and a drop voltage $V_{\rm d0}$ of a diode, the conduction losses in the 6 diodes of the full IGBT bridge is given by

$$\begin{aligned} P_{\rm d} &= 3\,I_{\rm m}\left(\frac{V_{\rm d0}}{\pi}+\frac{R_{\rm d}\,I_{\rm m}}{4}\right) \\ &- \frac{V_{\rm m}I_{\rm m}}{V_{\rm DC}}\cos(\phi_{\rm v/i})\left(\frac{V_{\rm d0}}{8}+\frac{R_{\rm d}I_{\rm m}}{3\,\pi}\right) \end{aligned} \quad (56)$$

For the switching losses and for a given maximal collector-emitter voltage $V_{\rm ce(max)}$, it is assume that the switching energy only depends on the absolute value of the current $I(t)$ and on the switched voltage $V_{\rm DC}$. Then, given a constant switching frequency $f_{\rm sw}$, the switching losses are [21]

$$p_{\rm sw}(t) = f_{\rm sw}\,k_{\rm esw}\,\frac{V_{\rm DC}}{V_{\rm ce(max)}}\,|I(t)| \quad (57)$$

where $k_{esw}$ is the switching energy constant (in $J.A^{-}1$) which depends on the IGBT voltage rating $V_{\rm ce(max)}$. From equation (57), the average switching losses on a period of the phase current $I(t)$ and for a 3-phases bridge is then given by [21] :

$$P_{\rm sw} = \frac{3}{\pi}\,f_{\rm sw}\,\frac{k_{\rm esw}}{V_{\rm ce\,max}}\,I_{\rm m}\,V_{\rm DC} \quad (58)$$

### 3.3.2. *Synthesis of IGBT and diode parameters*

To calculate the conduction and switching losses in a three phases IGBT bridge, different parameters must be defined. During the optimization of the complete flywheel system, many IGBT voltage and current rating could be tested. Then, it is useful to find relationship between the electrical parameters and the voltage and current capacities of IGBTs. In [8, 22], manufacturers' documentation are used to find the scale law of the main 3300 V-IGBT parameters. Here, this method is used and extended to a larger sample of IGBT with different voltage rating $V_{\rm ce(max)}$ (from 450 V to 6500 V) and different nominal current $I_{\rm cn}$ (from 50 A to 3600 A).

Figure 7 shows the scale law results for the switching energy constant $k_{\rm esw}$, the IGBT drop voltage $V_{\rm ce0}$ and the equivalent conduction resistance $R_{\rm c}$. It appears that the conduction resistance of the IGBT and diode only depend on the nominal current $I_{\rm cn}$. As for the drop voltages ($V_{\rm ce0}$ and $V_{\rm d0}$) and the switching energy constant ($k_{\rm esw}$), there only depend on the voltage rating $V_{\rm ce(max)}$. Next equations summarizes the scale law results for the full set of IGBT and diode parameters :

$$V_{\rm ce0} = V_{\rm d0} = 0.5+0.02\sqrt{V_{\rm ce(max)}} \quad (59)$$

$$R_{\rm c} = \frac{1.1}{I_{\rm cn}} \quad (60)$$

$$R_{\rm d} = \frac{0.8}{I_{\rm cn}} \quad (61)$$

$$k_{\rm esw} = 7\,10^{-12}\,V_{\rm ce(max)} \quad (62)$$

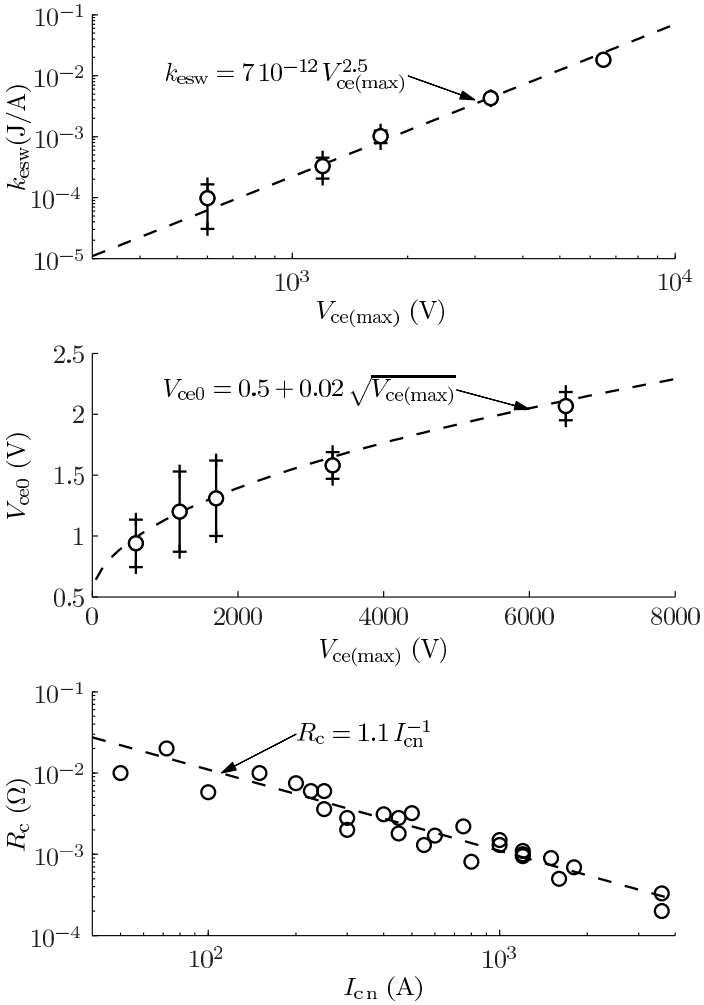


Fig. 7. Example of scale law results, obtained from manufacturers' document.

## 4. Economical models

In this work, the optimization of a flywheel energy storage system is base on a techno-economic approach. The section 3 deal with the physical models, defining the size and the electrical parameters of each subsystem. In this section, the economical models are presented. It include the acquisition and operating cost through the raw materials, lifetime and energy cost. The next subsection is dedicated to the acquisition cost of the flywheel, the PMSM and the power converter.

### *4.1. Acquisition costs*

Acquisition costs of the flywheel ($C_{\mathrm{FW}}$) and the PMSM ($C_{\mathrm{PMSM}}$) is based on the raw material quantity of steel, copper and magnet. The weight of iron, copper and magnet of the PMSM is obtained from equations (43), (44) and (47).

$$C_{\mathrm{PMSM}} = k_{\mathrm{dm}} \left( m_{\mathrm{mag}} \, C_{\mathrm{mag}} + m_{\mathrm{iron}} \, C_{\mathrm{iron}} + m_{\mathrm{co}} \, C_{\mathrm{co}} \right) \quad (63)$$

where $C_{\mathrm{mag}}$, $C_{\mathrm{iron}}$ and $C_{\mathrm{co}}$ are respectively the cost per kilogram of magnet, iron and copper. For PMSM ferromagnetic core and winding, commonly used materials are respectively the Fe-Si alloy and copper. Examples of cost values for these raw materials are given by table 1. These values are obtained or deduced from manufacturer's datas and literature [23, 24, 25]. An additional factor $k_{\mathrm{dm}}$ is introduced to include the cost of development and manufacturing, and is based on manufacturer's datas.

Tableau 1. Row material costs for the PMSM.

| Symbol | Description | System part | Value |
|---|---|---|---|
| $C_{\mathrm{iron}}$ | Fe-Si alloy | PMSM core | 3.0 €/kg |
| $C_{\mathrm{co}}$ | Copper | PMSM winding | 6.0 €/kg |
| $C_{\mathrm{mag}}$ | NdFeB | PMSM magnet | 140.0 €/kg |

For the flywheel, many materials can be used, with different mechanical properties [5, 26]. For high specific power applications (with mass constraints), composite materials such as Kevlar, R-Glass or E-Glass epoxy are well suited. The steel maraging has an high power to volume ratio and is then adapted to applications with volumic constraints. Table 2 gives the mechanical and economical characteristics for typical steel and composite materials. So, considering of flywheel with a mass $m_{\mathrm{fw}}$ and a cost

Tableau 2. Row material costs for the flywheel.

| Material | Density ($\mathrm{kg.m^{-3}}$) | Tensile Strength (MPa) | Cost €.$\mathrm{kg^{-1}}$ |
|---|---|---|---|
| 36NiCrMo16 | 7800 | 880 | 6 |
| Maraging 300 | 7800 | 1850 | 32.6 |
| E-Glass epoxy | 1900 | 1350 | 23.5 |
| R-Glass epoxy | 1550 | 1380 | 58.0 |
| Kevlar epoxy | 1370 | 1400 | 72.0 |

material $C_{\mathrm{material}}$, the final cost of the designed flywheel is given by :

$$C_{\mathrm{fw}} = k_{\mathrm{dfw}} \, m_{\mathrm{fw}} \, C_{\mathrm{material}} \quad (64)$$

where $k_{\mathrm{dfw}}$ is an additional cost factor, obtained from manufacturer's datas.

For the power converter, most works suggest cost based on the rated power. In [27, 28, 29, 30, 31, 32], the studied structures are dedicated to single phase inverter for grid connection of PV systems. They are well suited for the cost estimation of inverters with a rated power of 1 to 5 kW. There is, however, few studies on three-phase IGBT converters. In [33, 8], the authors deal with three phase AC-DC-AC converter for wind turbine, more expensive than a simple IGBT inverter. Additional datas are obtained from quotes of manufacturers, on three-phase IGBT inverters, including current sensors and DC-bus capacitor. These cost data are summarized in figure 8. The power converter cost (in €) can be

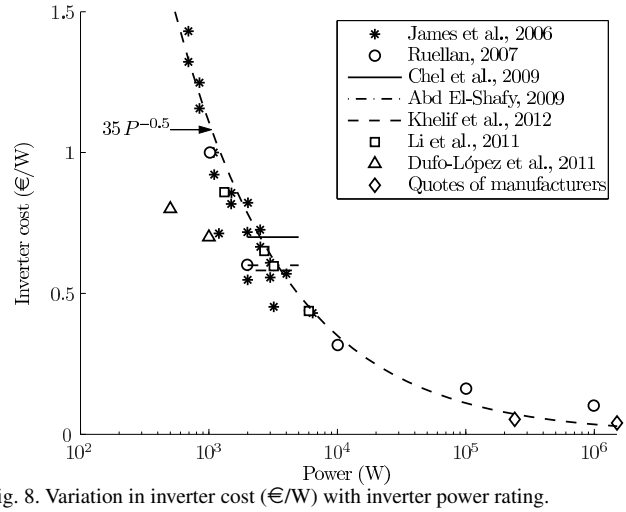


Fig. 8. Variation in inverter cost (€/W) with inverter power rating.

approximated from the trendline given figure 8 by :

$$C_{\mathrm{conv}} = 35 \, {P_{\mathrm{conv}}}^{0.5} \quad (65)$$

where $P_{\mathrm{conv}}$ is the maximal output power of the converter, obtained from rated voltage ($V_{\mathrm{ce(max)}}$) and current ($I_{\mathrm{c(max)}}$) of the IGBT :

$$P_{\mathrm{conv}} = \frac{3}{4} \, V_{\mathrm{ce(max)}} \, I_{\mathrm{c(max)}} \quad (66)$$

For IGBT, typical rated voltages are :

$$V_{\mathrm{igbt}} = \{400; 600; 1200; 1700; 3300; 4500; 6500 \, V\} \quad (67)$$

For the maximal current of IGBT devices, much more values exist. It is the reason why the computation of the power converter size is based on the maximal current $I_{\mathrm{m}}$ and on the rated voltage given by equation (67), directly above the selected DC-bus voltage $V_{\mathrm{DC}}$ :

$$V_{\mathrm{ce(max)}} = \min \left( V_{\mathrm{igbt}} > V_{\mathrm{DC}} \right) \quad (68)$$

$$I_{\mathrm{c(max)}} = I_{\mathrm{m}} \quad (69)$$

### 4.2. *Operating costs*

To be accurate, a techno-economic optimization on an electrical energy storage system must take into account the operating costs. The target application is a small electric ship, which carries short distances (round trip between two shores). Today, this ship exists and is only supplied with supercapacitors [11, 9, 10]. In this work, we compare this technological choice with a flywheel storage system, used as the only source of energy. The operating costs for such an application, must take into account the maintenance, the lifetime and the consumed electrical energy. In this work, the lifetime of the flywheel storage system is assumed to be 20 years. Because the maintenance few depends on the system sizing, it is not integrated in the optimization. However, the losses take a great part in the final cost of such a system. Total losses of the storage system, for one trip, is given by :

$$\begin{aligned} P_{\text{losses}}(t) &= P_{\text{co(avg)}} + P_{\text{mg(avg)}} + \\ & \quad P_{\text{igbt}}(t) + P_{\text{d}}(t) + P_{\text{sw}}(t) \end{aligned} \tag{70}$$

Considering a trip duration of $T_{\text{trip}}$, the lost energy $E_{\text{losses}}$ is then obtained by :

$$\begin{aligned} E_{\text{losses}} &= \left(P_{\text{co(avg)}} + P_{\text{mg(avg)}}\right) T_{\text{trip}} + \\ & \quad \int_0^{T_{\text{trip}}} P_{\text{igbt}}(t) + P_{\text{d}}(t) + P_{\text{sw}}(t) dt \end{aligned} \tag{71}$$

Because $E_{\text{losses}}$ is the total lost energy per trip, the cost energy on the lifetime of the boat is :

$$C_{\text{losses}} = C_{\text{kWh}}\, N_{\text{tpd}}\, 365\, LFT\, E_{\text{losses}} \tag{72}$$

with $N_{\text{tpd}}$ the number of trip per day, $LFT$ the lifetime in years of the solution and $C_{\text{kWh}}$ the cost for one kWh of electricity.

## 5. Optimization results

The optimization of the flywheel storage system is applied to the electrical ship *Ar Vag Tredan*, operating currently with ultracapacitors. The power cycle of each chain for one round-trip is illustrated by figure 9. It is assumed that the average number of crosses per day is 35 and a single crossing is made in 10 minutes plus a 5 minutes stop at each dock. But the ferry charges its supercapacitors only at the dock (R). The two objectives are the optimization of the total acquisition and operating cost for a duration of 20 years, and the volume of the storage system. Three materials for the flywheel (see Table 1) are tested and compared on the basis of these two criteria. The optimization variables are the maximum angular speed ($\Omega_{\text{max}}$) and the the inertia ($J$) of the flywheel, the number of turns of the PMSM ($n$). The rated current and voltage of the power converter are selected in a list of classical values (for IGBT devices). From the four input parameters and power cycle, the objective function implemented for this optimization must calculate the sum of acquisition and operation costs. The acquisition cost include the flywheel, the power converter and the electrical machine. The exploitation cost is the total lost energy during the 20 years of operation :

$$C_{\text{solution}} = C_{\text{conv}} + C_{\text{PMSM}} + C_{\text{fw}} + C_{\text{losses}} \tag{73}$$

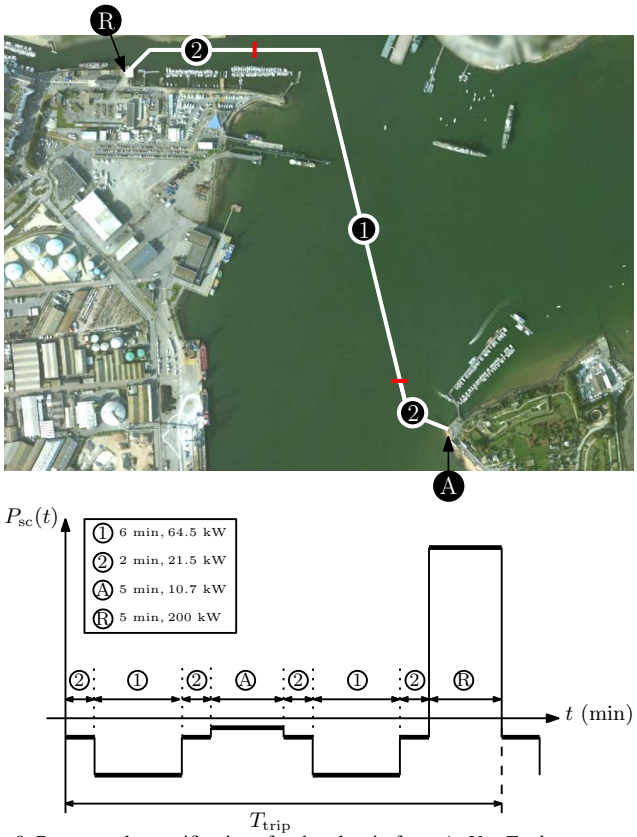


Fig. 9. Power cycle specifications for the plug-in ferry *Ar Vag Tredan*.

The volume of the storage system is calculated from the geometrical parameters of the flywheel and PMSM :

$$V_{\text{solution}} = \pi \left(R^2\, L + R_{\text{fw}}^2 L_{\text{fw}}\right) \tag{74}$$

Result is given as Pareto front on figure 10 and is obtained with the parameter set of table 3. This result shows that three materials used for the flywheel design permits to achieve a best set cost-volume. The Maraging material is expensive, but reduces the size of the storage system. In contrast, the E-glass leads to low-cost solutions, but constrained to a larger size for the flywheel. A balance is obtained with the R-glass composite material. The optimal cost of this energy storage system is between 80 and 200 k€, which gives a relative solution cost between 5 and 10 €/Wh, without the housing and accessories (vacuum chamber and magnetic bearing). In this application, the rms power is close to 100 kW and the useful energy per trip is of 16 kWh. These results can thus be compared to other works. In [34, 35, 36, 37], obtained values are of 1 to 4 €/W and 1 to 6 €/Wh, involving solution costs for this application between 80 and 500 k€. Three different flywheel sizing (one per material) are detailed in table 4 and illustrated in figure 12, corresponding to the three square markers of the figure 10.

For steel maraging and E-Glass composite materials, the maximum velocity is close to 20 krpm with a classical depth of discharge of 70 %. The main difference between these two solutions is the flywheel mass, three times greater for the steel maraging. In contrast, its volume is 20 % smaller, due to the high specific density of this material. Solution (3) with R-Glass com-

Tableau 3. List of used parameters for the optimization.

| | | |
|---|---|---|
| **Flywheel parameters** | | |
| $K_s$ | security factor | 0.9 |
| $K$ | shape factor | 0.606 |
| $k_{dfw}$ | Cost factor of manufacturing | 3.0 |
| **PMSM** | | |
| $\Delta T_{max}$ | temperature rising | 120 °C |
| $h$ | heat transfer coef. | 10 $W.m^{-2}K^{-1}$ |
| $p$ | number of pole pairs | 1 |
| $k_L$ | active length correction | 1.2 |
| $k_{f0}$ | winding fill factor per slot | 0.4 |
| $k_t$ | Slot opening to the tooth ratio | 0.5 |
| $k_{ad}$ | additional loss factor | 3.0 |
| $k_{ec}$ | eddy current loss coefficient | $6.5\,10^{-3}$ |
| $k_h$ | hysteresis loss coefficient | 15 |
| $r_w$ | Reduced outer winding radius | 0.73 |
| $r_s$ | Reduced inner stator radius | 0.73 |
| $\tau_L$ | Length to rotor radius ratio | 5.0 |
| $\rho_{co}$ | electric resistivity | $2.4\,10^{-8}$ Ω.m |
| $e$ | mechanical airgap | 4 mm |
| $e_{mag}$ | magnet height | 4 mm |
| $k_{dm}$ | Cost factor of manufacturing | 7.0 |
| **Power converter** | | |
| $f_{sw}$ | switching frequency | 10 kHz |
| **Other application settings** | | |
| $T_{amb}$ | ambiant temperature | 25 °C |
| $C_{kWh}$ | cost of electricity | 0.10 c€.$kWh^{-1}$ |
| $T_{trip}$ | travel time (round-trip) | 30 min |
| $E_u$ | useful energy of the round-trip | 16.6 kWh |
| $T_s$ | simulation sample time | 1 s |

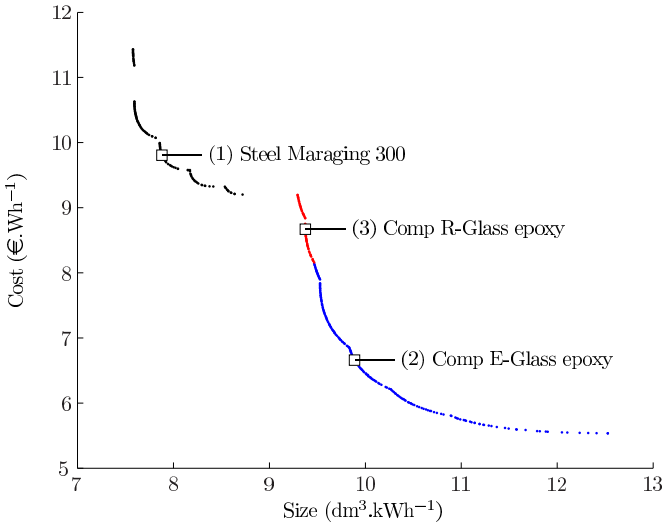

Fig. 10. Optimization results.

Tableau 4. Techno-economic optimization result for the three solutions (1-3).

| | Solution (1) | Solution (2) | Solution (3) |
|---|---|---|---|
| **Optimization variables** | | | |
| | Maraging 300 | E-Glass | R-Glass |
| $\Omega_{max}$ | 18.9 krpm | 18.9 krpm | 27.5 krpm |
| $J$ | 32.05 kg.m$^2$ | 32.05 kg.m$^2$ | 14.6 kg.m$^2$ |
| $n$ | 5 | 5 | 4 |
| **Flywheel** | | | |
| $\Omega_{min}$ | 30 %$\Omega_{max}$ | 30 %$\Omega_{max}$ | 24 %$\Omega_{max}$ |
| $R_{fw}$ | 0.31 m | 0.53 m | 0.41 m |
| $L_{fw}$ | 0.28 m | 0.13 m | 0.21 m |
| $m_{fw}$ | 671 kg | 224 kg | 172 kg |
| $v_{p(max)}$ | 613.2 m.s$^{-1}$ | 1061 m.s$^{-1}$ | 1188 m.s$^{-1}$ |
| **PMSM** | | | |
| $R$ | 0.18 m | 0.18 m | 0.18 m |
| $L$ | 0.39 m | 0.39 m | 0.39 m |
| $V_{pm(max)}$ | 155.6 m.s$^{-1}$ | 155.6 m.s$^{-1}$ | 223.6 m.s$^{-1}$ |
| $m_{iron}$ | 245 kg | 245 kg | 236 kg |
| $m_{co}$ | 28.4 kg | 28.3 kg | 27.4 kg |
| $m_{mag}$ | 1 kg | 1 kg | 0.76 kg |
| $\theta_{mag}$ | 33.4 ° | 33.4 ° | 25.8 ° |
| $\Gamma_{em(rms)}$ | 72.4 Nm | 72.3 Nm | 54.1 Nm |
| $\Omega_{(rms)}$ | 14.0 krpm | 14.0 krpm | 20.0 krpm |
| $\Omega_{(avg)}$ | 13.6 krpm | 13.6 krpm | 19.3 krpm |
| $P_{mg(avg)}$ | 383 W | 383 W | 374 |
| $P_{co(avg)}$ | 383 W | 383 W | 374 |
| $B_{fm(opt)}$ | 0.219 T | 0.219 T | 0.171 T |
| $R_{co}$ | 4.5 mΩ | 4.5 mΩ | 2.9 mΩ |
| $L_{cyc}$ | 569 $\mu$H | 568 $\mu$H | 356 $\mu$H |
| $k_\phi$ | 95.5 mV.rad$^{-1}$.s | 95.4 mV.rad$^{-1}$.s | 58.1 mV.rad$^{-1}$.s |
| **Power converter** | | | |
| $V_{ce(max)}$ | 1200 V | 1200 V | 1200 V |
| $I_{c(max)}$ | 1552 A | 1547 A | 2205 A |
| $V_{ce0}$ | 1.19 V | 1.19 V | 1.19 V |
| $R_c$ | 708 $\mu\Omega$ | 711 $\mu\Omega$ | 498 $\mu\Omega$ |
| $R_d$ | 515 $\mu\Omega$ | 517 $\mu\Omega$ | 362 $\mu\Omega$ |
| $k_{esw}$ | 350 $\mu$J.A$^{-1}$ | 350 $\mu$J.A$^{-1}$ | 350 $\mu$J.A$^{-1}$ |
| **Costs** | | | |
| Flywheel | 65.6 k€ | 15.8 k€ | 30.0 k€ |
| PMSM | 7.5 k€ | 7.4 k€ | 7.04 k€ |
| Converter | 56.3 k€ | 56.2 k€ | 72.0 k€ |
| Losses | 26.4 k€ | 26.4 k€ | 28.7 k€ |
| **TOTAL** | **155.8 k€** | **105.8 k€** | **137.7 k€** |
| **Volumes** | | | |
| Flywheel | 86.0 dm$^3$ | 118 dm$^3$ | 111.1 dm$^3$ |
| PMSM | 39.1 dm$^3$ | 39.1 dm$^3$ | 37.8 dm$^3$ |
| **TOTAL** | **125.2 dm$^3$** | **157.1 dm$^3$** | **148.9 dm$^3$** |
| Efficiency | 91.7 % | 91.8 % | 91.4 % |

posite material gives a maximum velocity of 27.5 krpm, and a depth of discharge of 75 %. This solution leads with a lightweight flywheel and a smaller machine, but requires a more powerful converter, because of the higher depth of discharge and the higher reactive power (due to the higher velocity).

Figure 11 shows the total cost sensitivity against the maximum velocity of the optimal solution. The cost of the machine and the flywheel decreases as the speed increases, which is a classical result in such system. Nevertheless, we show here that this trend is no longer true if one considers the losses and the power converter cost in the sizing. In solution (3), the additional cost of the losses and power converter is 20 % greater than the two lower velocity solutions (1) and (2).

Finally, these results can be compared to the supercapacitor solution given in [10]. For the same energy requirement and lifetime, the total cost of the supercapacitor storage system is

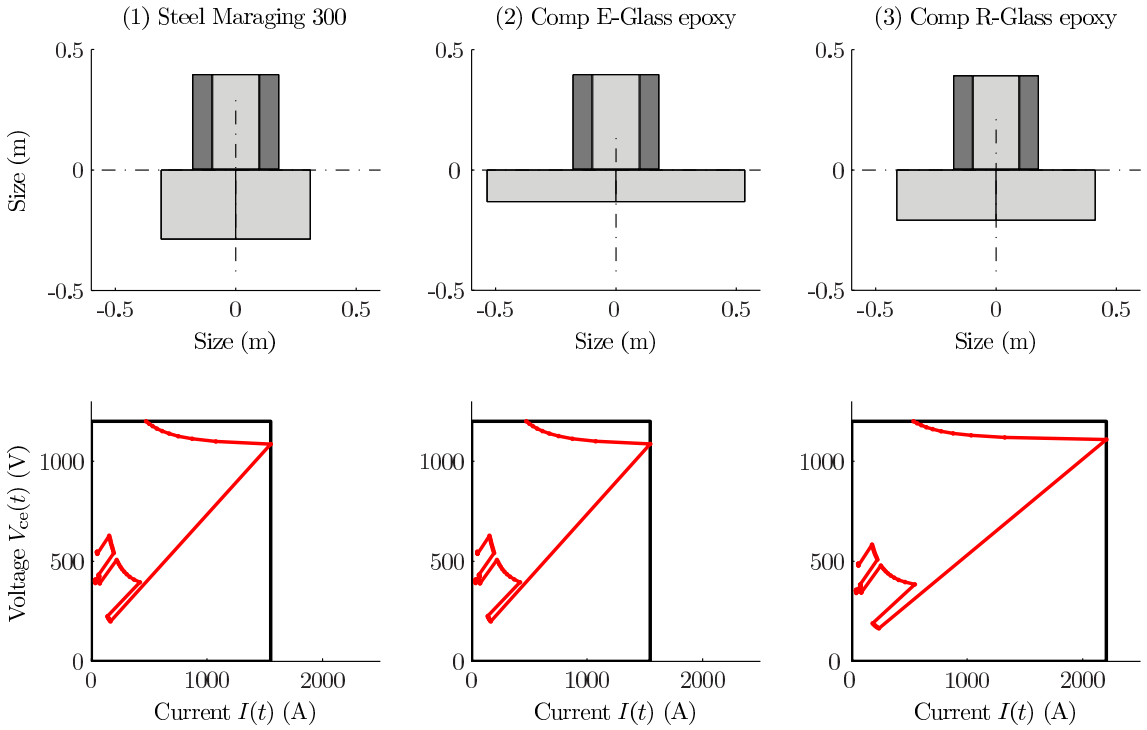


Fig. 12. Typical geometries and electrical cycles, obtained for each flywheel material.

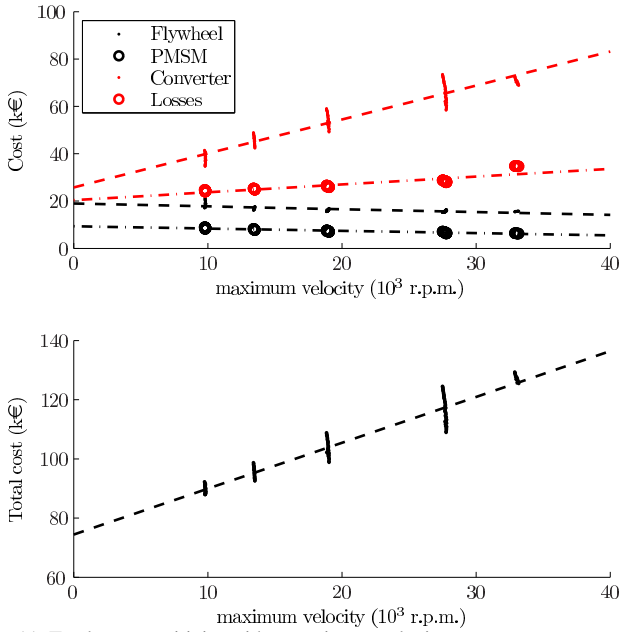


Fig. 11. Total cost sensitivity with a maximum velocity.

650 k€with a volume of 5 $m^3$ and a total weight of 4 000 kg (based on 4 $Wh.kg^{-1}$ and 3 $Wh.dm^{-3}$). Even if the total cost in this work do not take into account expensive accessories (magnetic bearings, vacuum chamber, ...), the cost of a supercapacitor solution is much more expensive, heavy and bulky. In contrast, flywheel storage system need additional safety caution and must include a compensation of gyroscopic effects.

## 6. Conclusion

This work present a methodology for the sizing of a flywheel storage system. Each subsystem is then described with technical and economical models, including the flywheel, the electrical machine and the power converter. The optimization is done for a set of three different flywheel materials and are compared on cost and size criteria, using the load profil of an ultracapacitor electrical ship, in operation since september 2013 in the harbor of Lorient. This work will show that a flywheel storage system is highly competitive with other technologies such as ultracapacitors or batteries. A next step of this work is to extend this study by adding various accessories such as magnetic bearings, which are necessary for long-terme storage.

## 7. References

[1] R. Sebastian and R. P. Alzola, "Flywheel energy storage systems : Review and simulation for an isolated wind power system," *Renewable and Sustainable Energy Reviews*, vol. 16, no. 9, pp. 6803 – 6813, 2012.

[2] N. Bernard, H. B. Ahmed, B. Multon, C. Kerzreho, J. Delamare, F. Faure, *et al.*, "Flywheel energy storage systems in hybrid and distributed electricity generation," *Proceeding PCIM 2003*, 2003.

[3] R. T. Doucette and M. D. McCulloch, "A comparison of high-speed flyw-

heels, batteries, and ultracapacitors on the bases of cost and fuel economy as the energy storage system in a fuel cell based hybrid electric vehicle," *Journal of Power Sources*, vol. 196, no. 3, pp. 1163 – 1170, 2011.

[4] F. Diaz-Gonzalez, A. Sumper, O. Gomis-Bellmunt, and R. Villafafila-Robles, "A review of energy storage technologies for wind power applications," *Renewable and Sustainable Energy Reviews*, vol. 16, no. 4, pp. 2154 – 2171, 2012.

[5] B. Bolund, H. Bernhoff, and M. Leijon, "Flywheel energy and power storage systems," *Renewable and Sustainable Energy Reviews*, vol. 11, no. 2, pp. 235 – 258, 2007.

[6] P. T. McMullen, L. A. Hawkins, C. S. Huynh, and D. R. Dang, "Design and development of a 100 kw energy storage flywheel for ups and power conditioning applications," in *24th International PCIM Conference*, (Nuremberg, Germany), May 20-22 2003.

[7] N. Bernard, F. Martin, and M. E.-H. Zaïm, "Design methodology of a permanent magnet synchronous machine for a screwdriver application," *Energy Conversion, IEEE Transactions on*, vol. 27, no. 3, pp. 624–633, 2012.

[8] J. Aubry, H. Ben Ahmed, and B. Multon, "Sizing optimization methodology of a surface permanent magnet machine-converter system over a torque-speed operating profile : Application to a wave energy converter," *IEEE Transactions on Industrial Electronics*, vol. 59, no. 5, pp. 2116–2125, 2012.

[9] S. Trieste, S. Bourguet, J.-C. Olivier, L. Loron, and J.-C. Le Claire, "Accurate sizing of supercapacitors storage system considering its capacitance variation," in *Power Electronics and Applications (EPE 2011), Proceedings of the 2011-14th European Conference on*, pp. 1–10, IEEE, 2011.

[10] S. Trieste, J.-C. Olivier, S. Bourguet, L. Loron, and D. Harpin, "Optimisation économique du dimensionnement d'un ensemble convertisseur-supercondensateurs utilisé pour l'énergie principale d'un véhicule électrique de type plug-in," in *14ème édition de la Conférence Electronique de Puissance du Futur*, Bordeaux, july 2012.

[11] *Passenger ship technology*. the international journal for cruise ships, ferries and fast ferries, 2012.

[12] R. Missoum, N. Bernard, M. E.-H. Zaïm, and J. Bonnefous, "Optimization of high speed surface mounted permanent magnet synchronous machines," in *Electrical Machines and Power Electronics, 2007. ACEMP '07. International Aegean Conference on*, pp. 446–451, 2007.

[13] M. Di Lella and R. Ramin, "Igbts for 3-level inverters, improved efficiency in dc/ac conversion," tech. rep., SEMIKRON, sep 2008.

[14] D. Graovac and M. Purschel, "Igbt power losses calculation using the datasheet parameters," Tech. Rep. Application Note 1.1, Infineon, Jan 2009.

[15] J. Shilling and G. Houze, "Magnetic properties and domain structure in grain-oriented 3% si-fe," *Magnetics, IEEE Transactions on*, vol. 10, no. 2, pp. 195–223, 1974.

[16] Z. Gmyrek, A. Boglietti, and A. Cavagnino, "Estimation of iron losses in induction motors : Calculation method, results, and analysis," *Industrial Electronics, IEEE Transactions on*, vol. 57, no. 1, pp. 161–171, 2010.

[17] J. Mühlethaler, J. Biela, J. Kolar, and A. Ecklebe, "Core losses under dc bias condition based on steinmetz parameters," in *IEEE International Power Electronics Conference*, pp. 2430–2437, 2010.

[18] A. Borisavljevic, H. Polinder, and J. Ferreira, "On the speed limits of permanent-magnet machines," *Industrial Electronics, IEEE Transactions on*, vol. 57, no. 1, pp. 220–227, 2010.

[19] A. Boglietti, A. Cavagnino, A. Tenconi, and S. Vaschetto, "Key design aspects of electrical machines for high-speed spindle applications," in *IECON 2010 - 36th Annual Conference on IEEE Industrial Electronics Society*, pp. 1735–1740, 2010.

[20] T. J. E. Miller, *Brushless Permanent-Magnet and Reluctance Motor Drives*. No. 21 in Monographs in electrical and electronic engineering, Oxford science publications, 1989.

[21] B. Backlund, R. Schnell, U. Schlapbach, R. Fischer, and E. Tsyplakov, "Applying igbts," Tech. Rep. 5SYA2053, ABB Switzerland Ltd, may 2012.

[22] J. Aubry, H. Ben Ahmed, and B. Multon, "Bi-objective sizing optimization of a pm machine drive on an operating profile," in *Electrical Machines (ICEM), 2010 XIX International Conference on*, 2010.

[23] W. Benecki, "A producer's and buyer's perspective : The per- a producerś and buyerś perspective : The permanent magnet outlook," in *Magnetics 2008 Conference*, (Denver, CO), may 2008.

[24] J. Aubry, P. Bydlowski, B. Multon, H. B. Ahmed, and B. Borgarino, "Energy storage system sizing for smoothing power generation of direct wave energy converters," in *3rd International Conference on Ocean Energy*, (Bilbao, Spain), October 2010.

[25] M. Pinilla and S. Martinez, "Optimal design of permanent-magnet direct-drive generator for wind energy considering the cost uncertainty in raw materials," *Renewable Energy*, vol. 41, no. 0, pp. 267 – 276, 2012.

[26] C. Kerzreho, *Caractérisation et optimisation d'une batterie électromécanique sous chargement cyclique*. PhD thesis, Cachan, Ecole normale supérieure, 2002.

[27] P. James, A. Bahaj, and R. Braid, "PV array $<$ 5 kwp + single inverter = grid connected PV system : Are multiple inverter alternatives economic ?," *Solar Energy*, vol. 80, no. 9, pp. 1179 – 1188, 2006.

[28] A. Chel, G. Tiwari, and A. Chandra, "Economic analysis of a stand-alone pv system to electrify a residential home in malaysia," *International Journal of Agile Systems and Management*, vol. 4, no. 1, pp. 21–40, 2009.

[29] A. N. Abd El-Shafy, "Design and economic analysis of a stand-alone pv system to electrify a remote area household in egypt," *The Open Renewable Energy Journal*, vol. 2, pp. 33–37, 2009.

[30] Z. Li, F. Boyle, and A. Reynolds, "Domestic application of solar PV systems in ireland : The reality of their economic viability," *Energy*, vol. 36, no. 10, pp. 5865 – 5876, 2011.

[31] R. Dufo-López, J. L. Bernal-Agustín, J. M. Yusta-Loyo, J. A. Domínguez-Navarro, I. J. Ramírez-Rosado, J. Lujano, and I. Aso, "Multi-objective optimization minimizing cost and life cycle emissions of stand-alone pv–wind–diesel systems with batteries storage," *Applied Energy*, vol. 88, no. 11, pp. 4033 – 4041, 2011.

[32] A. Khelif, A. Talha, M. Belhamel, and A. H. Arab, "Feasibility study of hybrid diesel–pv power plants in the southern of algeria : Case study on {AFRA} power plant," *International Journal of Electrical Power and Energy Systems*, vol. 43, no. 1, pp. 546 – 553, 2012.

[33] M. Ruellan, *Méthodologie de dimensionnement d'un système de récupération de l'énergie des vagues (in French)*. PhD thesis, Ecole Normale Supérieure de Cachan, Dec 2007.

[34] M. Y. Suberu, M. W. Mustafa, and N. Bashir, "Energy storage systems for renewable energy power sector integration and mitigation of intermittency," *Renewable and Sustainable Energy Reviews*, vol. 35, no. 0, pp. 499 – 514, 2014.

[35] R. Carnegie, D. Gotham, D. Nderitu, and P. V. Preckel, "Utility scale energy storage systems," 2013.

[36] Z. Zhou, M. Benbouzid, J. F. Charpentier, F. Scuiller, and T. Tang, "A review of energy storage technologies for marine current energy systems," *Renewable and Sustainable Energy Reviews*, vol. 18, no. 0, pp. 390 – 400, 2013.

[37] F. Rahman, S. Rehman, and M. A. Abdul-Majeed, "Overview of energy storage systems for storing electricity from renewable energy sources in saudi arabia," *Renewable and Sustainable Energy Reviews*, vol. 16, no. 1, pp. 274 – 283, 2012.